Pergamon

0956-7151(95)00224-3

Acta mater. Vol. 44, No. 3, pp. 1063–1076, 1996
Elsevier Science Ltd

1359-6454/96 $15.00 + 0.00

TRANSFORMATION-MISMATCH SUPERPLASTICITY IN REINFORCED AND UNREINFORCED TITANIUM

D. C. DUNAND† and C. M. BEDELL‡

Department of Materials Science and Engineering, Massachusetts Institute of Technology, Cambridge, MA 02139, U.S.A.

(Received 28 October 1994; in revised form 3 May 1995)

Abstract—Samples of commercial-purity titanium, with and without 10 vol.% TiC particulates, were thermally cycled about the allotropic transformation temperature of titanium. Thermal ratcheting was small for both unstressed materials. Upon application of an external uniaxial tensile stress, unreinforced titanium exhibited large strain increments, resulting from the biasing by the applied stress of the volume mismatch developed between grains during the transformation. Upon repeated cycling, a strain to fracture of 200% was reached, with a strain per cycle proportional to the external stress, in agreement with existing transformation-mismatch superplasticity models. The metal matrix composite displayed transformation-mismatch superplasticity as well, with a strain to fracture of 135% and a strain per cycle significantly higher than for unreinforced titanium. This novel enhancement of superplastic strain is modeled by considering the internal mismatch between the transforming matrix and the non-transforming particulates.

Résumé—Des échantillons de titane de pureté commerciale, avec ou sans 10 vol.% de particules de TiC, ont été cyclés thermiquement autour de la temperature de transformation allotropique du titane. La déformation sans contrainte externe est minime pour les deux matériaux. Sous contrainte externe en tension uniaxiale, le titane non-renforcé montre de grands incréments de déformation qui résultent du biaisage par la contrainte appliquée du désaccord de volume pendant la transformation. Après de multiples cycles, une élongation à la fracture de 200% a été atteinte, avec une déformation par cycle proportionelle à la contrainte externe, en accord avec des models existants de superplasticité par désaccord de transformation. Le composite à matrice métallique montre aussi de la superplasticité par désaccord de transformation, avec une élongation à la fracture de 135% et une déformation par cycle qui est nettement plus grande que celle du titane non renforcé. Ce nouvel effet est modellisé en considérant l'augmentation du désaccord interne dû à la présence de particules qui ne se transforment pas à l'intérieur d'une matrice qui se transforme.

Zusammenfassung—Proben, die aus komerziell reinem Titan sowie Titan mit 10 vol.% TiC Teilchen bestehen, wurden um die allotropische Umwandlungstemperatur von Titan thermischen Zyklen unterworfen. Die thermische Verschiebung im unbelasteten Zustand ergab sich als vernachlässigbar. Reines Titan zeigte unter einem einachsigem Spannungszustand eine beträchtliche Verformung, die auf eine Ueberlagerung der äusseren Last mit der durch den Volumenunterschied der transformierenden Körner auftretenden inneren Spannung zurückgeführt werden kann. Nach wiederholten thermischen Zyklen ergab sich eine Bruchverzerrung von 200%, wobei die Verzerrung pro Zylus proportional zur äusseren Spannung war, dies in Uebereinstimmung mit der Fachliteratur. Der Metall-Matrix Verbundwerkstoff zeigte ebenso Umwandlungsunterschiedsuperplastizität mit einer Bruchverzerrung von 135% und einer im Vergleich zu Titan deutlich erhöhten Verzerrung pro Zyklus. Dieser neuartige Effekt der Erhöhung der superplastichen Verzerrung wird in einem Modell, das auf dem Volumenunterschied der transformierenden Matrix mit den nicht-transformierenden Teilchen basiert, dargestellt.

1. INTRODUCTION

Superplasticity in metals can be induced by two types of mechanisms [1–3]: grain-boundary sliding in stable, fine-grained materials (microstructural superplasticity) and biasing of internal stresses or strains by an external stress (internal-stress superplasticity). For the latter type of superplasticity, internal stresses can be produced in polycrystalline materials by volume mismatch between grains, as a result of:

(i) anisotropic swelling upon irradiation, e.g. in uranium [4];

(ii) anisotropic coefficient of thermal expansion CTE (CTE-mismatch superplasticity), observed in, e.g. zinc, cadmium, zirconium and uranium [5–11];

(iii) density change upon phase transformation (transformation-mismatch superplasticity), observed in, e.g. titanium, zirconium, iron, cobalt and uranium [12–19].

If an external uniaxial stress is applied while the

†To whom all correspondence should be addressed.
‡Present address: Department of Civil and Mechanical Engineering, United States Military Academy, West Point, NY 10996, U.S.A.

volume mismatch exists, a net strain in the direction of the external stress results from the biasing of the internal stresses or strains [12]. Although the strain rate decays upon relaxation of the internal mismatch, the total strain is proportional to the externally-applied stress. Upon temperature cycling, the internal stresses are regenerated for mechanisms (i) and (ii) and additional strain increments are produced; the average strain rate is proportional to the applied stress, leading to a high resistance to necking and thus high strains to failure. These materials therefore behave in a superplastic manner, independently of their grain size, in sharp contrast to microstructurally-superplastic materials, which necessitate a stable, fine-grain structure [1–3].

Superplasticity in metal matrix composites is of particular interest, since these materials are typically difficult to form, due to their low ductility at both ambient and elevated temperature [20, 21]. Microstructural superplasticity can be achieved in metal matrix composites, if the matrix is inherently superplastic, or if the matrix exhibits very fine grains stabilized by the reinforcement [21–24]. As reviewed in Refs [21] and [25], internal-stress superplasticity can also be induced in composites by a mechanism similar to that operating in unreinforced metals with anisotropic thermal expansion [mechanism (ii) above]: when matrix and reinforcement exhibit different coefficients of thermal expansion, internal stresses are generated as a result of a temperature excursion. Upon thermal cycling with an external mechanical loading, CTE-mismatch superplasticity is observed in these metal matrix composites. The mismatching reinforcement can be in the form of particulates [26–32], whiskers [26, 33–41], short fibers [42–45], long fibers [46–48] and eutectic second phase [31, 49, 50].

In the present article, we investigate internal-stress superplasticity in a metal matrix composite, whereby the internal mismatch is induced by phase transformation of the matrix [mechanism (iii) above]. To the best of our knowledge, this is the first report of transformation-mismatch superplasticity in a composite. We compare the superplastic behavior of unreinforced titanium and titanium containing ceramic particulates, and discuss the results in the light of models based on biasing of internal strains and stresses.

2. EXPERIMENTAL PROCEDURES

Powders of commercially-pure, extra-low-chlorine titanium, with and without 10 vol.% equiaxed TiC particles of average size c. 20 μm, were consolidated into billets by cold-isostatic-pressing, followed by hot-isostatic-pressing. Processing conditions were 4 h at 1185°C at a pressure of 172 MPa for the composite billets, and 2 h at 900°C and a pressure of 103 MPa for the unreinforced billets. The resulting unreinforced and composite materials—respectively designated in what follows as CP–Ti and Ti–TiC—exhibited relative densities of at least 97 and 96%, respectively. Hourglass creep cylindrical specimens were machined to a gauge diameter of 6 mm and a gauge length of 30 mm. Parallelepiped samples 4 × 4 × 47 mm in size were used for thermal ratcheting experiments.

Constant load isothermal tensile creep experiments were performed at 1000°C under flowing high-purity, titanium gettered, argon gas, containing 4 ppm impurities (including 0.5 ppm oxygen). Sample elongation was measured with a linear voltage displacement transducer outside the hot-zone, and temperature was monitored by a thermocouple spot-welded to the sample gage length. After stabilizing the temperature, the sample was loaded and allowed to creep until a steady-state creep rate was reached. The sample was then subjected to a higher load, and again allowed to reach steady-state.

Tensile creep experiments under temperature cycling conditions were performed in the same apparatus used for isothermal creep measurements. Before cycling, steady-state creep was established at both the higher temperature of the cycle T_{max}, and the lower temperature of the cycle, T_{min}. The loaded sample was then subjected to temperature cycles about the transformation temperature of titanium, between T_{max} and T_{min}. Two cycle profiles were used (Fig. 1): a 12-min cycle between 830 and 960°C for CP–Ti, and a 15-min cycle between 830 and 1010°C for CP–Ti and Ti–TiC. Sample elongation was monitored during the whole cycle and sample strain was determined at the end of each hold period at T_{min}, thus eliminating the contribution of thermal expansion of sample and load train. A total of five to ten readable, error-free cycles were used to determine the average total strain per cycle $\Delta\epsilon_{tot}$ at a given stress. After cycling, steady-state creep at both T_{max} and T_{min} was again established. For a given sample, the above procedure was repeated for a total of at most five, monotonously increasing stress values. Finally, a sample with 35 mm gauge length was deformed up to fracture using a shortened 6-min cycle

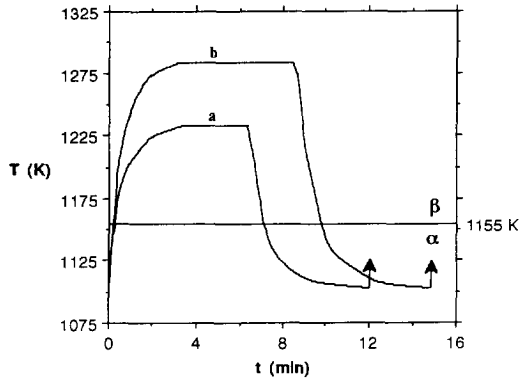

Fig. 1. Experimental thermal cycles: (a) low temperature cycle and (b) high temperature cycle.

between 830 and 1010°C, with a hold time of about 1.5 min at each of the extreme temperatures. For Ti–TiC a constant stress of 1.25 ± 0.05 MPa was maintained by periodic load adjustments, while for CP–Ti the stress increased monotonously from 1.2 to 1.6 MPa over the span of the experiment.

Thermal ratcheting experiments were carried out by placing samples in the hot-zone without applied stress, while the thermal cycling tests were taking place: the ratcheting samples were thus subjected to the same thermal cycling schedule as the creep samples. Sample length was measured after the first cycle and at longer intervals thereafter. Dilatometric experiments were performed by cycling a sample once between room temperature and 1000°C under flowing argon. The heating rate was 3 K min^{-1} from room temperature to 800°C and 1 K min^{-1} up to 1000°C, while the cooling rate was 0.2 K min^{-1} from 1000 to 700°C and 3 K min^{-1} down to room temperature.

3. RESULTS

Figure 2(a) and (b) shows the microstructure of as-received, undeformed CP–Ti and Ti–TiC samples, respectively. The somewhat porous TiC particles are well dispersed and exhibit in most cases a pore-free interface with the matrix. The grain size of CP–Ti samples is about 50 μm and the matrix grain size of Ti–TiC about 20 μm, as determined by the line-intercept method on etched samples. Since, for both samples, the grain size is above 10 μm, microstructural superplasticity can be ruled out [1–3].

In Fig. 3, the minimum strain rate is plotted as a function of the applied stress during isothermal creep at 1000°C for CP–Ti and Ti–TiC. Strain to failure for Ti–TiC at 1000°C was 30%, for a final stress of 3 MPa. Figure 4 shows the longitudinal ratcheting strain accumulated as a function of the number of thermal cycles with no applied load. For both CP–Ti and Ti–TiC, the strain after the first thermal cycle represents between 70 and 95% of the total ratcheting strain accumulated after 49–78 cycles. However, when cycled under load, both CP–Ti and Ti–TiC exhibit strains in the direction of the applied stress, which do not decay as the number of cycles is increased. Figure 5 shows the experimental average strain per cycle for CP–Ti cycled between 830 and 960°C and between 830 and 1010°C, which is proportional to the applied stress, as expected if transformation-mismatch superplasticity is taking place. Also plotted in Fig. 5 is the average strain per cycle for Ti–TiC for cycles between 830 and 1010°C. While the linear relationship between strain and applied stress also holds for the composite, Ti–TiC exhibits strains about 75% higher than those of CP–Ti at a given stress. As shown in Fig. 6, the total engineering strain to fracture ϵ_f is, however, smaller for Ti–TiC ($\epsilon_f = 135\%$) than for CP–Ti ($\epsilon_f = 200\%$, discounting about 20% elongation at the neck).

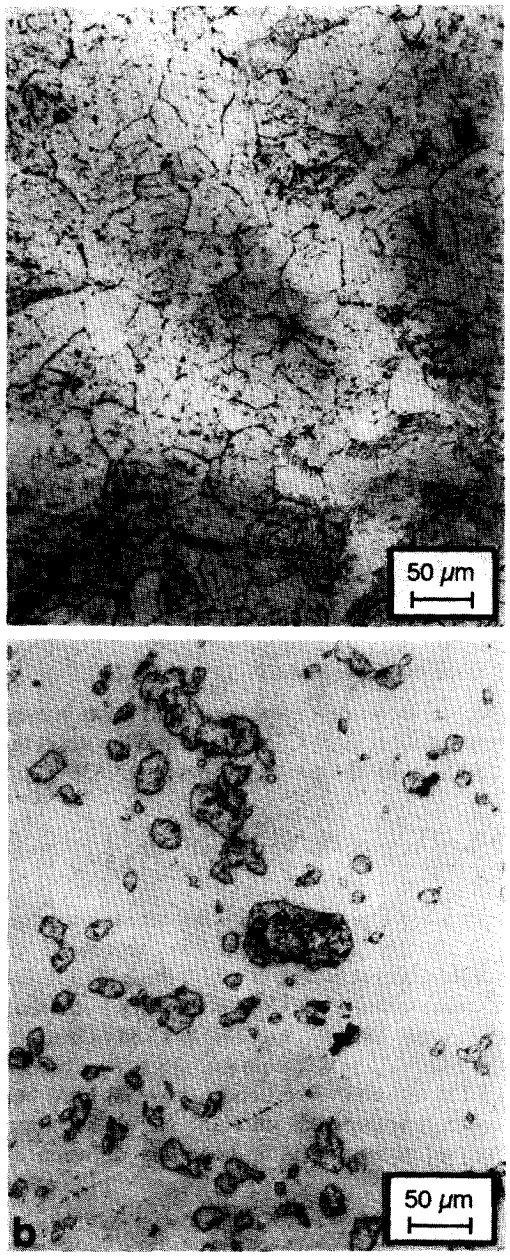

Fig. 2. Micrographs of undeformed (a) CP–Ti (Kroll's reagent) and (b) Ti–TiC (unetched).

The wide temperature interval used during cycling experiments was dictated by DSC results [51], which showed that the allotropic transformation of the matrix started at 930°C for Ti–TiC. Most likely, the matrix contained the α-stabilizing elements oxygen or nitrogen, which shift both $\alpha \rightarrow \alpha + \beta$ and $\alpha + \beta \rightarrow \beta$ transus temperatures to temperatures significantly higher than the allotropic transformation temperature of pure titanium ($T = 882$°C) [52]. In contrast, the start of the transformation of CP–Ti was measured at 880°C [51], indicating negligible contamination.

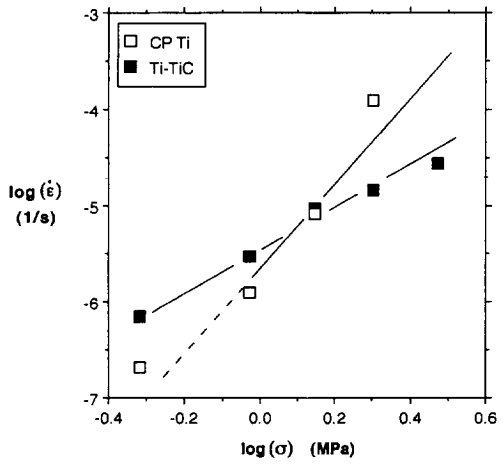

Fig. 3. Minimum strain rate for CP–Ti and Ti–TiC as a function of applied stress upon isothermal creep at 1000°C.

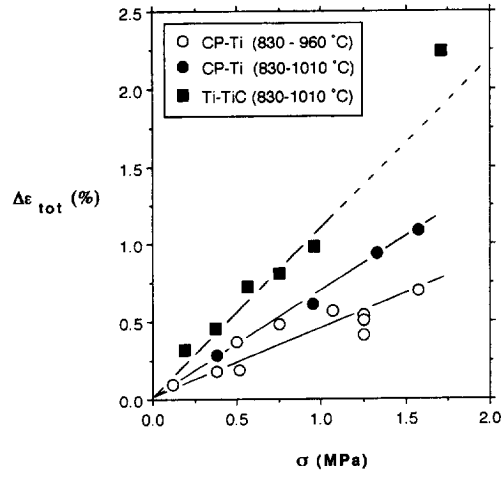

Fig. 5. Total measured strain per cycle $\Delta\epsilon_{tot}$ as a function of applied stress for CP–Ti and Ti–TiC.

4. DISCUSSION

4.1. Isothermal creep of CP–Ti and Ti–TiC

Figure 7 shows that good agreement exists between the creep data at 1000°C for CP–Ti and the strain rate $\dot{\epsilon}_{PL}$ predicted by the power-law equation [53]:

$$\dot{\epsilon}_{PL} = A \cdot D(T) \cdot \frac{G(T) \cdot b}{k \cdot T} \left(\frac{\sigma}{G(T)} \right)^n \qquad (1)$$

where σ is the applied stress, k is Boltzmann's constant and T is the temperature. The values of the pre-exponential constant, $A = 10^5$, the bulk diffusion coefficient at 1000°C, $D(1273) = 0.1\ \mu m^2 s^{-1}$, the shear modulus at 1000°C, $G(1273) = 15.34$ GPa, the Burgers vector $b = 0.286$ nm and the stress exponent $n = 4.3$, are given by Frost and Ashby [53]. Only bulk diffusion is considered, since the calculated contributions of pipe- and grain-boundary diffusion are found to be negligible [53]. Also shown in Fig. 7 are creep data measured on β-Ti at low stresses—at 982°C by Lunsford and Grant [54] and at 1002°C by Oikawa *et al.* [55]—which are in satisfactory agreement with our results. Equation (1) is furthermore plotted in Fig. 7 with materials constants by Oikawa *et al.* [55] ($A = 8 \times 10^4$ and $n = 4.1$), slightly different from those of Frost and Ashby [53]. Our data are in better agreement with equation (1) if the materials constant from the latter authors are selected, which we use for the calculations to follow.

The stress and grain size ranges are low enough that diffusional creep $\dot{\epsilon}_D$ must also be taken into account [53]:

$$\dot{\epsilon}_D = \frac{14 \cdot \Omega \cdot D(T)}{k \cdot T \cdot d^2} \sigma \qquad (2)$$

where $\Omega = 0.0181\ nm^3$ is the atomic volume and d is the grain size. The sum of the contributions of power-law and diffusional creep $\dot{\epsilon}_{PL} + \dot{\epsilon}_D$ [equation (1) and equation (2)] is plotted in Fig. 7. The stress for which the contributions of each mechanism are equal is $\sigma = 0.65$ MPa, corresponding to the boundary between power-law creep and diffusional creep in Frost and Ashby's deformation mechanism map [53]. The effective stress exponent in the vicinity of this border changes from $n = 1$ (diffusional creep) to $n = 4.3$ (power-law creep).

In the relatively narrow stress range $\sigma = 0.5$–3 MPa, the stress exponent of Ti–TiC at 1000°C is $n = 2.2$ (Fig. 3). Such a low value is unexpected, since most metal matrix composites in the power-law regime exhibit an apparent stress exponent which is larger than that of the unreinforced matrix [21]. This low value of stress exponent may however correspond to the transition between diffusional flow and power-law creep mentioned above, which is indeed expected to take place at higher stresses for Ti–TiC than for CP–Ti, due to the smaller grain size of the composite.

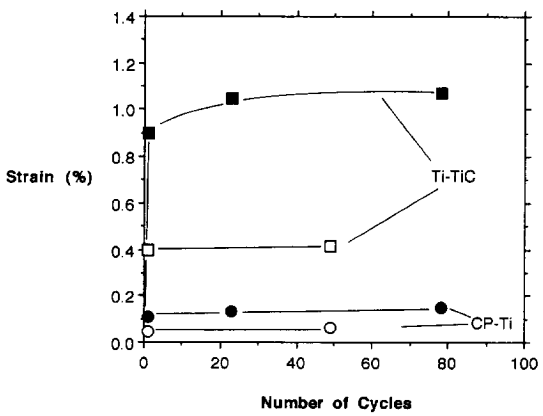

Fig. 4. Cumulative ratcheting longitudinal strain as a function of the number of cycles for cycling experiments without applied stress. Two samples were measured for CP–Ti and Ti–TiC each.

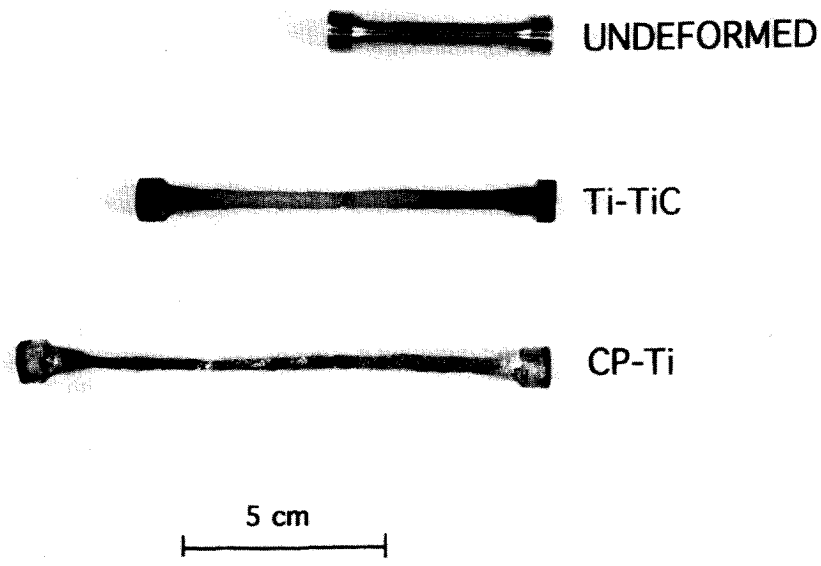

Fig. 6. Thermally-cycled samples deformed to fracture. CP–Ti: 200% strain for a stress of 1.4 ± 0.2 MPa. Ti–TiC: 135% strain for a stress of 1.25 ± 0.05 MPa.

4.2. Transformation-mismatch superplasticity of CP–Ti

Thermal cycling experiments with no applied stress show that most of the longitudinal deformation is accumulated after the first cycle (0.047–0.11%, Fig. 4) and is thus most probably the result of relaxation of residual stresses. After the first cycle, however, the ratcheting strain per cycle (about 4×10^{-4} %) is much smaller than the constrained transformation strain of 1.6% [56], as also reported for uranium and iron cycled through their phase transformation [17, 57]. Assuming that a well-defined transformation front travels longitudinally through the sample and that the weaker phase deforms plastically in the directions parallel to the front, the cycled allotropic metal expands (respectively shrinks) longitudinally if the stronger phase has a larger (respectively smaller) density [17, 57]. Because α-titanium is stronger and less dense than β-titanium [53, 56] and because the transformation front is expected to be parallel to the faces of the parallelepiped specimens, longitudinal expansion is predicted during ratcheting, in agreement with observation (Fig. 4).

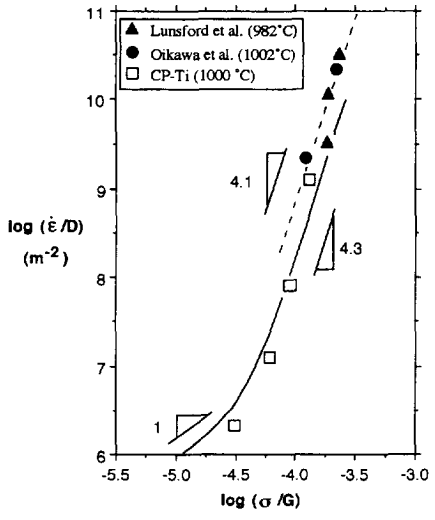

Fig. 7. Comparison of isothermal creep data at 1000°C for CP–Ti with results by Lunsford and Grant [54] ($T = 982$°C) and by Oikawa *et al.* [55] ($T = 1002$°C). The sum of equations (1) and (2) is plotted with materials constants by Frost and Ashby [53] (solid line) and equation (1) is plotted with constants by Oikawa *et al.* [55] (dotted line).

In contrast to the very small ratcheting strains, the longitudinal strain resulting from thermal cycling under an applied load is large, up to 1.1% per cycle (Fig. 5), and strain increments can be added after each cycle without decaying. Fracture was observed after an engineering strain of 220% (200% if the necked region is not considered) under a constant stress of 1.4 MPa. Both the high resistance to necking, and the linear relationship between strain per cycle and applied stress (Fig. 5), indicate that CP–Ti exhibits transformation-mismatch superplasticity. The total strain measured after one cycle (Fig. 5) is the sum of both superplastic strains and strains accumulated as a result of power-law creep outside the transformation temperature. To determine the contribution $\Delta\epsilon$ due to transformation superplasticity alone, the strain $\Delta\epsilon_{PL}$, resulting from power-law creep during the temperature cycle, is subtracted from the total measured strain $\Delta\epsilon_{tot}$:

$$\Delta\epsilon = \Delta\epsilon_{tot} - \Delta\epsilon_{PL}. \quad (3)$$

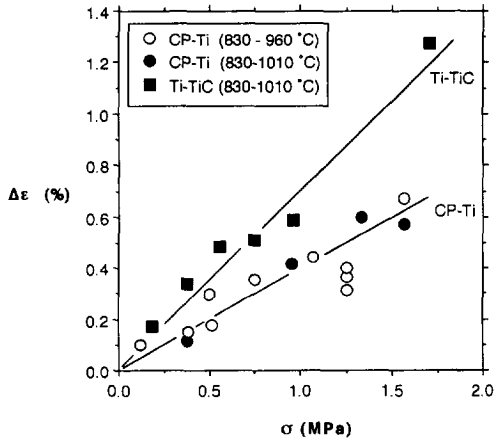

Fig. 8. Superplastic strain per cycle $\Delta\epsilon$ as a function of the applied stress for data presented in Fig. 5.

The strain $\Delta\epsilon_{PL}$ is determined by averaging the strain rate due to power-law creep over the temperature range spanned during the cycle:

$$\Delta\epsilon_{PL} = \Delta t \cdot \dot{\epsilon}_{max} \cdot \frac{D_{eff}}{D(T_{max})} \tag{4}$$

where $\dot{\epsilon}_{max}$ is the experimental steady state creep at T_{max} (taken as the average of the two values measured before and after cycling), Δt is the duration of the cycle, $D(T_{max})$ is the diffusion coefficient at the temperature T_{max} and D_{eff} is the effective diffusion coefficient, averaged over the temperature spanned during one cycle [5]:

$$D_{eff} = \frac{1}{\Delta t} \int_0^{\Delta t} D_o \exp\left(-\frac{Q}{RT(t)}\right) dt. \tag{5}$$

In equation (5), $T(t)$ is the experimental heating profile (Fig. 1), R is the gas constant and D_o and Q are, respectively, the pre-exponential constant and the activation energy for lattice diffusion, given in Ref. [53] for α-Ti and β-Ti. Graphical integration of equation (5) yields $D_{eff} = 3.12 \times 10^{-14}$ m^2 s^{-1} for cycles between 830 and 960°C, and $D_{eff} = 6.75 \times 10^{-14}$ m^2 s^{-1} for cycles between 830 and 1010°C. The effective temperatures corresponding to these effective diffusion coefficients are $T_{eff} = 905$°C and $T_{eff} = 966$°C, respectively. They represent the temperatures at which the isothermal strain rate due to power-law creep would be equal to the strain rate averaged over the temperature cycle. Figure 8 shows the superplastic strain per cycle $\Delta\epsilon$ after correction according to equation (3). There is little difference between the superplastic strains per cycle for the two cycling profiles used for CP–Ti, despite the significantly higher isothermal creep contribution $\Delta\epsilon_c$ for the high-temperature cycle (Fig. 5), which is thus correctly calculated by equation (4).

Using the Levy–von Mises criterion and considering the biasing of internal strains by the externally applied stress σ, Greenwood and Johnson [12] derived a relationship for the strain $\Delta\epsilon_t$ due to transformation plasticity over a complete cycle:

$$\Delta\epsilon_t = \frac{5}{3} \frac{\Delta V}{V} \frac{\sigma}{\sigma_y} \tag{6}$$

where $\Delta V/V$ is the fractional constrained volume change during the transformation and σ_y is the uniaxial yield stress of the weakest phase at the transformation temperature. Since creep is rapid for β-Ti at 882°C, we follow Greenwood and Johnson's approach to determine the yield stress. We take the flow stress $\sigma(\dot{\epsilon}^*)$ given by equation (1), where $\dot{\epsilon}^*$ is the rate at which the sample is deformed, which is estimated as the uniaxial transformation strain $\Delta V/3V$ divided by the time Δt^* for the transformation to take place:

$$\dot{\epsilon}^* = \frac{1}{3} \frac{\Delta V}{V} \frac{1}{\Delta t^*}. \tag{7}$$

Using the value $\Delta V/V = 4.8 \times 10^{-3}$ measured by McCoy [56] and the experimental value $\Delta t^* \approx 160$ s, Equation (7) yields $\dot{\epsilon}^* \approx 10^{-5}$s^{-1}, and equation (1) gives for the yield stress $\sigma_y \approx \sigma(\dot{\epsilon}^*) = 2.0$ MPa. equation (6) then predicts a value $\Delta\epsilon_t/\sigma = 4.0$ GPa^{-1}, in good agreement with the experimental value $\Delta\epsilon/\sigma = 4 \pm 0.5$ GPa^{-1} (Fig. 8). We use the value of $\Delta\epsilon$ determined from equation (3), rather than the measured value $\Delta\epsilon_{tot}$, since equation (6) does not take into account the contribution of power-law creep accumulated during the cycle and superimposed to the biased superplastic strain [equation (3)]. We note that equation (6) is valid for $\Delta\epsilon_t < 2 \cdot (\Delta V/V) = 9.6 \times 10^{-3}$ [12], a condition which is met in Fig. 8, where the largest experimental value is $\Delta\epsilon = 6.7 \times 10^{-3}$.

If the weakest phase is deforming by time-dependent power-law creep, rather than time-independent yield, Greenwood and Johnson [12] considered the biasing of internal stresses, rather than the biasing of the internal strains leading to equation (6), and derived a related expression:

$$\Delta\epsilon_t = \frac{4}{3} \cdot \frac{\Delta V}{V} \cdot \frac{5n}{4n+1} \cdot \frac{\sigma}{\sigma_{int}} \tag{8}$$

where σ_{int} is the internal stress generated during the phase transformation and n is the stress exponent. With $\sigma_{int} = \sigma(\dot{\epsilon}^*) = 2.0$ MPa and $n = 4.3$, equation (8) predicts a value $\Delta\epsilon_t/\sigma = 3.8$ GPa^{-1} close to that predicted by equation (6) and observed experimentally. Equation (8) is however only valid for $\sigma_{int} \gg \sigma$, and can thus only be compared to the data measured at low applied stresses.

Also considering biasing of an average internal stress σ_i, Wu *et al.* [5] derived an equation for the average strain rate $\dot{\epsilon}_{tot}$, by assuming that half of the dislocations experience a stress which is increased by the internal stress $(\sigma + \sigma_i)$, and the other half

experience a stress which is reduced by the internal stress ($\sigma - \sigma_i$):

$$\dot{\epsilon}_{tot} = \frac{1}{2}\left[\dot{\epsilon}(|\sigma + \sigma_i|) + \frac{|\sigma - \sigma_i|}{\sigma - \sigma_i}\dot{\epsilon}(|\sigma - \sigma_i|)\right] \quad (9)$$

where $\dot{\epsilon}(\sigma)$ is the functional creep relationship. Equation (9) can be approximated by a linear relationship, when the internal stress σ_i is significantly greater than the applied stress σ. For a power-law material deforming according to equation (1), the low-stress regime is described by:

$$\dot{\epsilon}_{tot} = n \cdot \dot{\epsilon}(\sigma_i) \cdot \frac{\sigma}{\sigma_i} \quad (10)$$

where n is the power-law stress exponent. Taking the average strain rate $\dot{\epsilon}_{tot}$ as the measured cycling strain, $\Delta\epsilon_{tot}$, multiplied by the cycling frequency, equation (10) yields $\sigma_i = 1.03$ MPa, using $T_{eff} = 966°C$ as the effective temperature for the 15 min cycles between 830 and 1010°C. For the data from the 12-min cycles between 830 and 960°C, a fit of equation (10) gives $\sigma_i = 1.22$ MPa, i.e. higher than the value found for the 15 min cycles. Wu *et al.* [5] also found an increase in internal stress with decreasing maximal temperature and increasing cycling frequency. We note that the internal stress according to Greenwood and Johnson [12], $\sigma_{int} = 2$ MPa, and according to Wu *et al.* [5], $\sigma_i = 1.03$–1.22 MPa, cannot be directly compared, since the former authors perform a multiaxial stress analysis, while the latter consider only uniaxial stresses. Finally, while the calculated internal stress values are on the order of the experimental applied stress values, equation (10) is only valid for the low range of applied stress values in Fig. 5. Using equation (9) with the internal stress values fitted above, a significant divergence between the predicted and the measured data is found above stress values on the order of 0.7 MPa.

Figure 9 compares the measured strain per cycle, $\Delta\epsilon$, corrected for isothermal creep according to equation (3), with results from other experiments reported in the literature for pure titanium. The superplastic strain per cycle measured by Greenwood and Johnson [12] ($\Delta\epsilon/\sigma = 9$ GPa^{-1}) is significantly higher than our value $\Delta\epsilon/\sigma = 4 \pm 0.5$ GPa^{-1}, probably because these authors did not correct for power-law creep during the cycle [equation (3)]. This may also explain why their data does not intersect the origin when extrapolating with a linear dependence between stress and strain, since the power-law creep contribution increases according to equation (1) with $n = 4.3$. Our data ($\Delta\epsilon/\sigma = 4 \pm 0.5$ GPa^{-1}) are in reasonable agreement with results by Kot *et al.* [13] ($\Delta\epsilon/\sigma = 2.6$ GPa^{-1}) for titanium tested in tension at a rate of 14–28 K s^{-1} and with measurements by Furushiro *et al.* [16] ($\Delta\epsilon/\sigma = 5$ GPa^{-1}), performed in compression at a rate of 0.05 K s^{-1}. The latter authors found that the strain per cycle was dependent on both the cycle frequency and the orientation of the applied stress with respect to the rolling direction of their samples. Chaix and Lasalmonie [14] however found a higher value ($\Delta\epsilon/\sigma = 8$ GPa^{-1}) upon testing in compression at a rate of 0.03 K s^{-1}. Possible reasons for this discrepancy are examined below. First, Chaix and Lasalmonie [14] tested titanium samples machined from sheets, which were probably rolled; the resulting texture may have influenced the measured strain, as shown by Furushiro *et al.* [16]. On the other hand, our samples were fabricated by hot-isostatic-pressing of powders and are thus expected to be texture-free. Second, the correction for power-law creep rate was performed differently in the two studies. Third, the specimens of Chaix and Lasalmonie [14] were almost monocrystalline after cycling, and thus may have shown very anisotropic mismatch stresses. Our samples however exhibited negligible grain growth, possibly as a result of impurities from powder processing, which pinned the grain boundaries. Finally, Chaix and Lasalmonie [14] did not pre-creep their samples prior to the thermal cycling experiments. We have found that, under these conditions, the strain per cycle in the first few cycles was significantly higher than if the sample had reached steady-state creep prior to cycling. This effect can be explained by a non-negligible contribution of primary creep to $\Delta\epsilon_{PL}$.

Another related issue is the effect of the allotropic transformation upon the steady-state creep of titanium: if the phase transformation eliminates the dislocation substructure developed upon steady-state creep, primary creep is expected to take place after each crossing of the allotropic transformation temperature. This would lead to a larger value of $\Delta\epsilon_{PL}$ than calculated using equation (3), which is based on steady-state strain rates, and thus to a lower value of

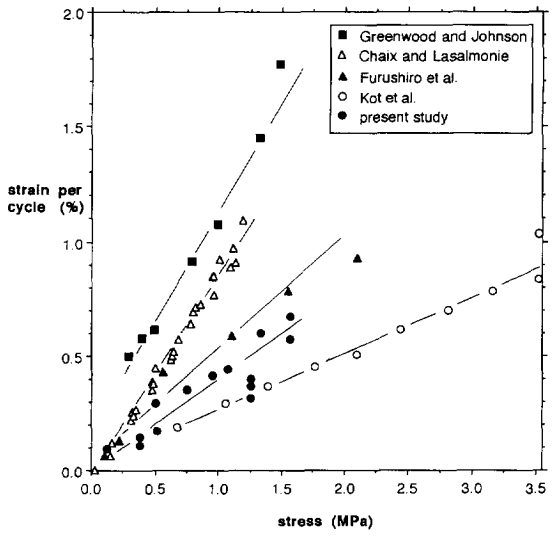

Fig. 9. Superplastic strain per cycle upon α–β–α cycling of pure titanium as a function of applied stress: data from Greenwood and Johnson [12], Chaix and Lasalmonie [14], Furushiro *et al.* [16] (average of 3–4 data points), Kot *et al.* [13] (average of 2 points, except at highest stress) and CP–Ti (present study).

the calculated strain per cycle $\Delta\epsilon$. The following experiment was performed on CP–Ti to examine this issue. First, the unstressed sample was heated to 950°C, loaded to a stress of 1 MPa and the steady-state creep rate measured. The sample was then unloaded, cooled below the transformation temperature to 800°C, reheated to 950°C and reloaded to the same stress. The measured creep rate at 950°C was similar to that before the temperature excursion, indicating that primary creep was negligible after the transformation.

4.3. *Transformation-mismatch superplasticity of Ti–TiC*

Like CP–Ti, samples of Ti–TiC cycled about the phase transformation of the matrix without applied stress develop most of their longitudinal strain after the first cycle (Fig. 4), indicating relaxation of internal stresses, probably as a result of sample machining. This is confirmed by the dilatometry data of an as-machined specimen [51], exhibiting a large deviation from the CTE dilation curve at temperatures above about 550°C upon heating, but no such anomaly upon cooling. The initial large strain increment in Fig. 4 is not due to transformation or CTE-residual stresses, since it is not observed after any of the subsequent cooling to room-temperature, performed for length measurement for each of the data point in Fig. 4. For one of the Ti–TiC samples shown in Fig. 4, thermal ratcheting after the first cycle is comparable to that of CP–Ti (3.5×10^{-4} % per cycle). For the other Ti–TiC sample, with the largest elongation after the first cycle in Fig. 4, the average ratcheting rate is markedly larger up to cycle 23, but similar to that of CP–Ti between cycle 49 and cycle 78 (3.5×10^{-4} % per cycle). We conclude that, at steady-state, thermal ratcheting is not increased by the titanium carbide particles, as expected from the isotropic average mismatch resulting from equiaxed particles. However, as reviewed in Ref. [21], CTE-mismatch ratcheting in whiskers-reinforced composite is observed if the whiskers are aligned, as a result of anisotropic relaxation of internal stresses.

In contrast to the ratcheting experiments described above, temperature cycling of Ti–TiC with an applied external stress leads to large strain increments of up to 2.25% per cycle (Fig. 5), independently of the number of cycles. Upon repeated cycling, these increments can be added up to high values without premature failure: a total engineering strain to fracture $\epsilon_f = 135\%$ was measured under a constant stress of 1.25 MPa. For comparison, the strain to failure for Ti–TiC is significantly smaller for isothermal creep at 1000°C ($\epsilon_f = 30\%$, for a final stress of 2.96 MPa). The strain to failure under thermal cycling is however less for Ti–TiC ($\epsilon_f = 135\%$) than for CP–Ti ($\epsilon_f = 200\%$), suggesting that the TiC particles accelerate fracture by cavitation, as also observed in composites deformed by fine-grain superplasticity [22]. The large tensile strains and the linear relationship between strain per

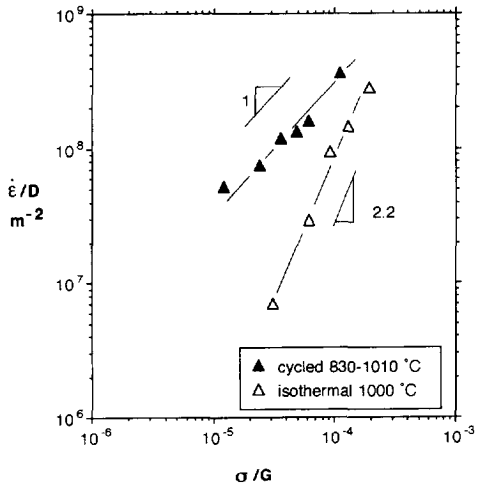

Fig. 10. Normalized strain rates as a function of stress for Ti–TiC deformed under cycling and isothermal conditions.

cycle and stress (Fig. 5) indicate that Ti–TiC is deforming superplastically when subjected to both external loading and thermal cycling about the allotropic transformation temperature of the matrix. To the best of our knowledge, this is the first report of transformation-mismatch superplasticity in a metal matrix composite.

Figure 10 compares the normalized strain rates for Ti–TiC deformed under cycling and isothermal conditions, respectively. For the cycling experiments, the total strain accumulated during the cycle $\Delta\epsilon_{tot}$ divided by the cycle time Δt is taken as the average strain rate. The diffusion coefficient and the shear modulus at $T = 1000$°C and $T_{eff} = 966$°C are used to normalize the data under isothermal and cycling conditions, respectively. It is apparent from Fig. 10 that, at low stresses, the effective strain rate of Ti–TiC under thermal cycling conditions is significantly higher than under isothermal conditions, even for the relatively low cycling frequency used in the present study. This suggests that transformation-mismatch superplasticity could be used in forming operations for titanium-based composites, similarly to the forming of aluminum composites by CTE-mismatch superplasticity demonstrated by Chen *et al.* [39].

The mechanism responsible for superplastic deformation is expected to be similar for both expansion- and transformation-mismatch composite superplasticity, i.e. biasing of internal stresses or strains induced by volume mismatch between the matrix and the reinforcement. However, there are significant differences between these two types of superplasticity. First, in the case of transformation-mismatch superplasticity, the temperature (or temperature interval) at which the deformation can take place is dictated by the thermodynamic stability of the transforming phase; the temperature interval for CTE-mismatch superplasticity can be varied within broad limits, giving more flexibility to the latter process. Second, the expansion-mismatch developed

in a composite is proportional to the temperature interval spanned during the cycle, while the whole transformation mismatch occurs at a constant temperature (for a pure metal) or within the temperature range at which the two allotropic phases coexist (for an alloy). In both cases, however, the mismatch developed is proportional to the heat flowing into, or out of, the sample. In the latter case, the transformation enthalpy ΔH_t is proportional to the volumetric transformation mismatch $\Delta V/V$, while in the former case the enthalpy $C_p\Delta T$ (which is necessary to change by ΔT the temperature of the composite with specific heat C_p) is proportional to the volumetric CTE mismatch $3\Delta\alpha\Delta T$, where $\Delta\alpha$ is the CTE difference between the two phases. The dimensionless number ρ:

$$\rho = \frac{\frac{\Delta V}{V}\cdot C_p}{3\cdot\Delta\alpha\cdot\Delta H_t} \tag{11}$$

then corresponds to the ratio of the enthalpy necessary to induce a given mismatch by thermal expansion, to the enthalpy needed to induce a mismatch of the same magnitude by allotropic transformation. For example, this ratio is about $\rho = 4$ for the system Ti–TiC and $\rho = 13$ for the system Fe–TiC, using thermodynamic and physical values given in Refs [58–60]. Thus, for a given mismatch, cycling outside the transformation temperature requires 4 (respectively 13) times more enthalpy than cycling at the transformation temperature. If, as a first approximation, we assume that a given mismatch results in a given superplastic strain per cycle, independently of the source of the mismatch, then the cycling frequency (and the average strain rate that can be reached upon superplastic forming) will be higher by a factor ρ for transformation-mismatch superplasticity than for CTE-mismatch superplasticity for a given heat flux (i.e. heating system). The above approximation is a lower bound for the strain-rate advantage of composite transformation-mismatch superplasticity since, as shown below, the strain per cycle of a composite deformed by transformation-mismatch superplasticity is the sum of the strain observed in the matrix alone (ignored in the above discussion) and the strain induced by matrix-reinforcement mismatch.

Finally, while CTE-mismatch superplasticity is applicable to the majority of metal–ceramic combinations, transformation-mismatch superplasticity is, by the very nature of its mechanism, limited to composites exhibiting a mismatch-inducing phase transformation [61]. Metallic matrices of technological interest exhibiting an allotropic transformation at ambient pressure include metals (e.g. beryllium, titanium, iron, cobalt, zirconium, tin, uranium [52]), alloys based on these allotropic metals (e.g. steels and Ti–6Al–4V) as well as intermetallic compounds of non-allotropic metals (e.g. $MoSi_2$, Ni_4Si, Cr_2Nb [52]). Zirconia and bismuth-containing oxides are examples of allotropic ceramics showing transformation superplasticity [62, 63] which, in combination with a non-transforming ceramic or metallic phase, could exhibit composite transformation superplasticity. Reference [64] lists further metallic and non-metallic materials exhibiting allotropic phase transformations at ambient pressure. Finally, because most metals [65] and many ceramics [66] exhibit allotropic phases at elevated pressure, composite transformation-mismatch superplasticity by pressure-cycling is not only possible in principle, but may be relevant for geological materials subjected to high pressures [67], for instance allotropic silicates containing non-allotropic inclusions in the earth mantle.

4.4. Modeling of enhanced transformation-mismatch superplasticity in Ti–TiC

As shown in Fig. 8, the superplastic strain without power-law creep contribution is significantly higher for Ti–TiC ($\Delta\epsilon/\sigma = 7 \pm 0.5$ GPa^{-1}) than for the CP–Ti ($\Delta\epsilon/\sigma = 4 \pm 0.5$ GPa^{-1}). This novel effect is particularly noteworthy, since metal matrix composites typically exhibit lower creep rates than their unreinforced matrix [21], as also observed in the present study for Ti–TiC at stresses above 1.5 MPa at 1000°C (Fig. 3). We hypothesize that the strain enhancement observed upon cycling of the composite is due to the increased internal mismatch in the matrix, as a result of the non-transforming particles.

We first examine two other possible mechanisms which may explain the enhancement observed in Figs 5 and 8. First, we note that the matrices of CP–Ti and Ti–TiC start to transform at 880 and 930°C, respectively. The yield stress of β-Ti given by equations (1) and (7) are $\sigma_y = 2$ MPa and $\sigma_y = 1.7$ MPa at these respective temperatures. Equation (6) then predicts for the matrix a superplastic strain higher by a factor $2/1.7 = 1.18$ at the higher transformation temperature, a factor which is significantly smaller than the observed strain enhancement factor of 1.75 between CP–Ti and Ti–TiC (Fig. 8). Also, while contamination by oxygen (and thus the transformation temperature) increased with the duration of the experiments (as illustrated by the Widmannstatten structure observed in cycled titanium samples [51]), the measured strains per cycle were not found to increase with time, indicating that the above effect is not important. Another possible explanation for the observed enhancement in Ti–TiC is the difference of CTE between the two phases, which is expected to result in CTE-mismatch superplasticity. Averaged between 830 and 1010°C, the CTE of titanium and TiC are respectively $\alpha_{Ti} = 11.4 \times 10^{-6}$ K^{-1} and $\alpha_{TiC} = 8.6 \times 10^{-6}$ K^{-1} [58, 59], corresponding to a volumetric mismatch due to CTE differences, $3(\alpha_{TiC}-\alpha_{Ti})\Delta T = -1.5 \times 10^{-3}$. The magnitude of this mismatch is significantly smaller than that of the density mismatch upon transformation, $\Delta V/V = 4.8 \times 10^{-3}$ [56] and the signs of the mismatches are opposite: a volume contraction is observed upon heating through the transformation from the low-temperature α-phase to the high temperature

β-phase [56, 58, 59, 68], while a volume expansion results from the thermal expansion. The CTE mismatch is therefore canceled by the larger transformation mismatch. We conclude that the observed enhancement of superplastic deformation of Ti–TiC cannot be explained by CTE-mismatch superplasticity. In what follows, we examine the effect on superplastic deformation of internal stresses resulting from the transformation of titanium in the presence of an inert, non-transforming second-phase.

As discussed earlier, both CTE mismatch and transformation mismatch induce internal stresses in a similar manner, and models for composite CTE-mismatch superplasticity are thus applicable with a few modifications to the present problem. Biasing of strains or stresses has been invoked by most authors modeling composite CTE-mismatch superplasticity, whereby the internal mismatch has been determined by continuum mechanics [28, 33, 37, 38, 45, 49, 50, 69], by the Eshelby method [41–44] or by finite elements [32, 35, 70]. While models taking into account the biasing of internal strains by the external stress are appropriate for systems which do not exhibit significant creep deformation as a result of the internal stresses, these models are difficult to apply to the present case, since the yield stress is ill-defined due to rapid creep of β-Ti at the transus temperature. Such a strain-biasing model is presented in the Appendix and predicts a superplastic strain enhancement which is in rough agreement with the measured effect for Ti–TiC. In what follows, we examine creep models based on the biasing of internal stresses, which are more applicable to a rapidly-creeping system such as Ti–TiC.

Fitting the experimental data for Ti–TiC (Fig. 5) to equation (10) derived by Wu *et al.* [5] yields an internal stress $\sigma_i = 1.22$ MPa, which is higher than the value $\sigma_i = 1.02$ MPa found above for CP–Ti under the same cycling conditions. While the model is not predictive and can only be used at low applied stresses, the magnitude of the internal stress in the composite is reasonable, since it is below the yield stress of the matrix as defined above. In another model, Furness and Clyne [42, 43] used the Eshelby method [71, 72] to calculate the average deviatoric stresses in the matrix resulting from the superposition of the external applied stress and the internal CTE-mismatch stresses from oriented short fibers. Since in Ti–TiC the particles are assumed spherical and the volume transformation mismatch is assumed isotropic, this model predicts a purely hydrostatic spatial-average matrix stress and therefore no enhancement of the creep rate for the composite.

Recently, Sato and Kuribayashi [69] have developed a multiaxial model for composite CTE-mismatch superplasticity, which takes into account the spatial variation of the state of stress within the matrix. Unlike models based on the Eshelby method, their model thus predicts volume-averaged deviatoric stresses in the matrix for the case of a mismatching elastic sphere. They assume that the matrix deforms according to a multiaxial power-law equation, and that interfacial diffusion relaxes the inclusion deviatoric back-stresses created by the incompatibility between the creeping matrix and the elastic inclusion. Upon thermal cycling with constant heating/cooling rate $\dot{T}$, the uniaxial steady-state average strain rate $\bar{\dot{\epsilon}}$ is then predicted as:

$$\bar{\dot{\epsilon}} = \frac{2n(n+4)}{2^{1/n}5} \cdot \frac{(1-f^{1/n})}{(1-f)^2} \cdot (f \cdot \dot{\epsilon}_{mis})^{1-1/n} \cdot \dot{\epsilon}(\sigma)^{1/n} \quad \text{for } \sigma \ll \sigma(\dot{\epsilon}_{mis}) \quad (12a)$$

$$\bar{\dot{\epsilon}} = (1-f)^{-n} \dot{\epsilon}(\sigma) \quad \text{for } \sigma \gg \sigma(\dot{\epsilon}_{mis}) \quad (12b)$$

where σ is the biasing stress, $\dot{\epsilon}(\sigma)$ is described by the uniaxial power-law given by equation (1), n is the corresponding stress exponent, f is the volume fraction inclusions and the rate of internal mismatch strain between matrix and particulate is:

$$\dot{\epsilon}_{mis} = |\Delta\alpha \cdot \dot{T}|. \quad (13)$$

At low applied stresses, the strain rate is proportional to stress [equation (12a)], while at high applied stresses, a power-law behavior is predicted [equation (12b)].

Unlike CTE-mismatch superplasticity of composites such as Al–SiC, the matrix of which is not superplastic upon thermal cycling, the matrix of Ti–TiC exhibits transformation-mismatch superplasticity without the presence of reinforcement (Figs 5 and 8). The matrix superplastic strain is thus enhanced by the presence of the non-transforming carbide particles by an increment $\Delta\epsilon/\sigma$(Ti–TiC) $-$ $\Delta\epsilon/\sigma$(CP–Ti) $= 4 \pm 1$ GPa^{-1} (Fig. 5). As a first-order approximation, we assume that the two effects—superplastic strain of the unreinforced titanium matrix and superplastic strain from the mismatch between the transforming matrix and the inert reinforcement—can be added linearly. We can then treat the strain enhancement effect by the mismatching TiC particles within the superplastic titanium matrix in a similar fashion as the enhancement effect of a mismatching reinforcement in a non-superplastic, non-transforming matrix (CTE-mismatch superplasticity). Using the model by Sato and Kuribayashi [69] described above, we assume that the mismatch strain rate for Ti–TiC can be averaged as:

$$\dot{\epsilon}_{mis} = \frac{1}{\Delta t}\left(\left|\frac{1}{3}\frac{\Delta V}{V}\right| \pm |\Delta\alpha\Delta T'|\right) \quad (14)$$

where $\Delta T' = 1283 - 1203 = 80$ K is the magnitude of the temperature excursion above the transformation temperature and $\Delta t = 300$ s is the time for the heating portion of this excursion. We note that the contribution of the transformation mismatch $\Delta V/3V = 1.6 \times 10^{-3}$ is significantly larger than that of the CTE mismatch $\Delta\alpha\Delta T' = 2.2 \times 10^{-4}$. If these two mismatch strains are added in equation (14), an upper bound for the total mismatch strain upon heating is

found, corresponding to a system with mismatches of the same sign. Alternatively, for a system such as Ti–TiC with mismatches of opposite signs, the two contributions can only be added if they take place sequentially and if the relaxation of internal stresses is rapid [69]: for example, a pure metal exhibiting an isothermal transformation, followed by a temperature increase where only CTE mismatch strains are created. If however the two contributions are subtracted in equation (14), a lower bound is found, corresponding to the case where the transformation mismatch develops over the whole temperature interval (i.e. for an alloy with its two-phase region spanning the temperature interval $\Delta T'$), concurrently with a thermal expansion mismatch of opposite sign, which partially cancels the transformation mismatch.

We take the time average of equation (12) for the total average strain over a half cycle:

$$\Delta\bar{\epsilon} = \int_0^{\Delta t} \bar{\epsilon}[T(t)]\,\mathrm{d}t \tag{15}$$

where the temperature cycle is approximated by a triangular wave, the first half of which is given by:

$$T(t) = T_0 + \Delta T' \cdot \frac{t}{\Delta t} \tag{16}$$

where $T_0 = 1203$ K (930°C) is the transformation start temperature in the composite.

As shown by Sato and Kuribayashi [69] and as reflected by the use of absolute values in equations (13) and (14), $\dot{\epsilon}_{mis}$ does not depend on the sign of the mismatching strains: the sign of the uniaxial steady-state average strain rate $\bar{\epsilon}$ of the sample is thus expected to be the same upon heating and cooling. Neglecting the transient due to the reversal of strain direction at T_{max} and T_{min}, the total strain per cycle due to the presence of TiC particles therefore is $2\Delta\bar{\epsilon}$. The superplastic strain of the composite $\Delta\epsilon_c$ is then:

$$\Delta\epsilon_c = \Delta\epsilon_{Ti} + 2\Delta\bar{\epsilon} \tag{17}$$

where $\Delta\epsilon_{Ti}$ is the superplastic strain of the unreinforced matrix.

We first examine the low-stress regime, for which a linear relationship exists between applied stress and strain rate [equation (12a)]. Introducing equations (12a), (14) and (16) into equation (15), and solving numerically with the material constants of β-Ti given above, yields $2\Delta\bar{\epsilon}/\sigma = 2.34 - 2.9$ GPa^{-1}. With this value and the measured value of the superplastic strain of CP–Ti $\Delta\epsilon_{Ti}/\sigma = 7 \pm 0.5$ GPa^{-1} (Fig. 5), equation (17) yields $\Delta\epsilon_c/\sigma = 9.6 \pm 0.8$ GPa^{-1}, in satisfactory agreement with the superplastic strain $\Delta\epsilon/\sigma = 11 \pm 1$ GPa^{-1} measured at low stresses (Figs 5 and 11). The contribution of CTE-mismatch superplasticity for the interval 830–930°C is negligible: using $\Delta t = 150$ s and equations (12a), (13) and (15), we find $2\Delta\bar{\epsilon}/\sigma = 0.11$ GPa^{-1}.

For the high stress regime, equations (12b) and (14)–(17) are solved as described above, assuming the same linear relationship for the superplastic strain of CP–Ti ($\Delta\epsilon_{Ti}/\sigma = 7 \pm 0.5$ GPa^{-1}), found valid in Fig. 5 for stresses up to 1.57 MPa. The resulting non-linear relationship between applied stress and strain per cycle predicted for the composite is also plotted in Fig. 11 and found to be in reasonable agreement with the data point for Ti–TiC measured at high applied stress ($\sigma = 1.71$ MPa).

Many simplifying assumptions have been made in the above analysis. First, we have assumed that the transformation strain of the pure matrix could be added to the mismatch strain due to the particles [equation (17)]. We in effect assumed that the stresses are localized, either at the boundary between two matrix grains or at the interface between a matrix grain and a particle. Second, the temperature profile is assumed triangular [equation (16)], and does not correspond closely to the experimental profile given in Fig. 1. However, the temperature profile within the sample bulk is likely to be closer to the triangular shape assumed in equation (16) than Fig. 1 is, since the transformation enthalpy absorbed or released by the sample during cycling flattens the slopes of the heating and cooling ramps. Third, the model assumes equal elastic moduli for both phases and small inclusion volume fraction; this will introduce errors in the internal stress determination, since these conditions are not met. Fourth, the transformation mismatch between matrix and particle [equation (14)] is assumed to be equivalent to a CTE mismatch of the same magnitude [equation (13)]. At the microscopic level, however, the mismatch is quite different in nature: for CTE mismatch, the strains are isotropic and generated along the whole particle–matrix interface, as assumed in the original model. Transformation mismatch is however likely to be more localized, depending on the location of the transforming grains. The use of average stress values may however limit this error. Fifth, the

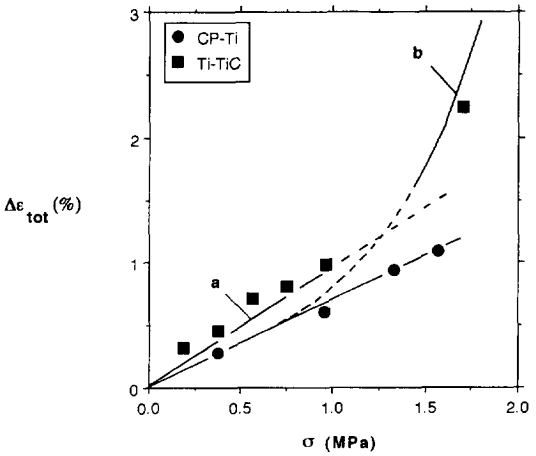

Fig. 11. Total strain per cycle $\Delta\epsilon_{tot}$ as a function of applied stress σ, measured for CP–Ti and Ti–TiC cycled between 830 and 1010°C. Predicted strain for Ti–TiC (a) at low stresses from equations (12a) and (17) and (b) at high stresses from equations (12b) and (17).

angular shape of the particles, which may result in locally higher stress, is not taken into account. However, as shown by Withers *et al.* [73], these stress concentrations can be ignored at a short distance from the interface (Saint-Venant's principle). Finally, interfacial diffusion, assumed to be rapid in the above model, is found to be very slow when using the estimation given in Ref. [69] for the Ti–TiC system at $T_{eff} = 966°C$ for particles 5 μm in radius. Other relaxation mechanisms, such as interfacial sliding, prismatic loop punching or enhanced diffusion by local stress concentration, may however allow the relaxation of deviatoric stresses in the particles. Despite the above approximations and the uncertainty linked with the materials constants used, the agreement between the predicted superplastic strain increase, calculated above using equation (17) without disposable parameters, and the observed superplastic deformation for the composite is satisfactory (Fig. 11). We thus conclude that the enhancement of superplastic deformation observed in the composite can be quantitatively described by the biasing of the internal stresses in the transforming matrix, which are increased by the inert, non-transforming TiC particles.

5. CONCLUSIONS

Isothermal creep of commercial-purity titanium (CP–Ti) and titanium containing 10 vol% TiC equiaxed particles (Ti–TiC) was measured at 1000°C for stresses between 0.4 and 3 MPa. The creep behavior of CP–Ti is well predicted by power-law creep with a stress exponent $n = 4.3$. The stress exponent for Ti–TiC is 2.2, indicative of a regime intermediate between power-law and diffusion control.

Thermal ratcheting upon cycling about the allotropic transformation temperature of titanium with no external stress applied is small for CP–Ti (4×10^{-4} % per cycle). Except for transients in the first cycles, the same ratcheting value is found for Ti–TiC, as expected since the equiaxed reinforcement induces an isotropic mismatch with the matrix.

Thermal cycling about the transformation temperature under an applied uniaxial stress induces transformation-mismatch superplasticity in CP–Ti. For applied stresses between 0.19 and 1.72 MPa, the strain per cycle $\Delta\epsilon$ varies linearly with the applied stress σ as $\Delta\epsilon/\sigma = 4\ GPa^{-1}$ (without power-law creep contribution). This value is in good agreement with the model by Greenwood and Johnson [12] considering the biasing by the external stress of the internal strain induced by the density mismatch between transforming grains. Fracture occurs at a strain of 200% under a constant stress of 1.4 MPa.

The composite Ti–TiC exhibits transformation-mismatch superplasticity in the same stress range, with a strain to failure of 135% for a stress of 1.25 MPa. To the best of our knowledge, this is the first report of transformation superplasticity for a metal matrix composite. Superplastic forming of Ti–TiC and other composites exhibiting a phase transformation is thus possible, independently of the grain size of the materials [61].

The superplastic strain per cycle for Ti–TiC ($\Delta\epsilon/\sigma = 7\ GPa^{-1}$, without power-law creep contribution) is significantly higher than for CP–Ti. This novel effect is modeled by considering the increase of internal stresses in the creeping matrix as a result of the mismatch between the transforming matrix and the non-transforming particles. The superplastic strain per cycle predicted by the biasing of internal stresses is in satisfactory agreement with the observed superplastic strains of the composite.

Acknowledgements—This research was supported by the Materials Processing Center at MIT. CMB and DCD gratefully acknowledge the support of the U.S. Army, in the form of a graduate fellowship, and of AMAX, in the form of an endowed chair at MIT, respectively. The authors also express their appreciation to Dynamet Technology Inc. (Burlington, MA) for providing billets, to Mr P. Zwigl from MIT for performing the two superplastic tests to fracture, to Professor A. S. Argon from MIT for use of experimental facilities and to Dr B. Derby from the University of Oxford for helpful discussions.

REFERENCES

1. J. Pilling and N. Ridley, *Superplasticity in Crystalline Solids*. The Institute of Metals, London, U.K. (1989).
2. K. A. Padmanabhan and G. J. Davies, *Superplasticity*. Springer, London (1980).
3. J. W. Edington, K. N. Melton and C. P. Cutler, *Prog. Mater. Sci.* **21**, 61 (1976).
4. A. C. Roberts and A. H. Cottrell, *Phil. Mag.* **1**, 711 (1956).
5. M. Y. Wu, J. Wadsworth and O. D. Sherby, *Metall. Trans.* **18A**, 451 (1987).
6. S. M. Pickard and B. Derby, *Scripta metall. mater.* **25**, 467 (1991).
7. B. Derby, *Superplasticity in Metals, Ceramics and Intermetallics* (edited by M. J. Mayo, M. Kobayashi and J. Wadsworth), p. 115. MRS (1990).
8. W. Boas and R. W. K. Honeycombe, *Proc. R. Soc. Lond.* **186A**, 57 (1946).
9. W. Boas and R. W. K. Honeycombe, *Proc. R. Soc. Lond.* **188A**, 427 (1947).
10. R. H. Johnson and R. W. K. Honeycombe, *J. Less Common Metals* **4**, 226 (1962).
11. R. C. Lobb, E. C. Sykes and R. H. Johnson, *Metal Sci. J.* **6**, 33 (1972).
12. G. W. Greenwood and R. H. Johnson, *Proc. R. Soc. Lond.* **283A**, 403 (1965).
13. R. Kot, G. Krause and V. Weiss, *The Science, Technology and Applications of Titanium* (edited by R. I. Jaffe and N. E. Promisel), p. 597. Pergamon Press, Oxford (1970).
14. C. Chaix and A. Lasalmonie, *Res Mech.* **2**, 241 (1981).
15. Y. Takayama, N. Furushiro and S. Hori, *Titanium Science and Technology* (edited by G. Lutjering, U. Zwicker and W. Bunk), p. 753. Deutsche Gesellschaft für Metallkunde (1985).
16. N. Furushiro, H. Kuramoto, Y. Takayama and S. Hori, *Trans. ISIJ* **27**, 725 (1987).
17. M. de Jong and G. W. Rathenau, *Acta metall.* **7**, 246 (1959).

18. F. W. Clinard and O. D. Sherby, *Acta metall.* **12,** 911 (1964).
19. M. Zamora and J. P. Poirier, *Mech. Mater.* **2,** 193 (1983).
20. A. Mortensen, *Fabrication of Particulate Reinforced Metal Composites* (edited by J. Masounave and F. G. Hamel), p. 217. ASM International, Metal Park, OH (1990).
21. D. C. Dunand and B. Derby, *Fundamentals of Metal Matrix Composites* (edited by S. Suresh, A. Mortensen and A. Needleman), p. 191. Butterworth–Heinemann, Boston, MA (1993).
22. A. K. Ghosh, *Fundamentals of Metal Matrix Composites* (edited by S. Suresh, A. Mortensen and A. Needleman), p. 23. Butterworth–Heinemann, Boston, MA (1993).
23. K. Higashi and M. Mabuchi, *Advanced Composites* '93 (edited by T. Chandra and A. K. Dhingra), p. 35. TMS, Warrendale, PA (1993).
24. J. Wadsworth and T. G. Nieh, *Mater. Sci. Engng* **A166,** 97 (1993).
25. B. Derby, *Metal Matrix Composites—Processing, Microstructure and Properties* (edited by N. Hansen, D. Juul-Jensen, T. Leffers, H. Lilholt, T. Lorentzen, A. S. Pedersen, O. B. Pedersen and B. Ralph), p. 31. Risø National Laboratory, Roskilde, Denmark (1991).
26. J. C. LeFlour and R. Locicero, *Scripta metall.* **21,** 1071 (1987).
27. S. M. Pickard and B. Derby, *9th Risø Int. Symp. on Metallurgy and Materials Science* (edited by S. I. Andersen, H. Lilholt and O. B. Pedersen), p. 447. Risø National Laboratory, Roskilde, Denmark (1988).
28. S. M. Pickard and B. Derby, *Acta metall. mater.* **38,** 2537 (1990).
29. S. M. Pickard and B. Derby, *Fundamental Relationship Between Microstructure and Mechanical Properties of Metal Matrix Composites* (edited by P. K. Liaw and M. N. Gungor), p. 103. TMS, Warrendale, PA (1990).
30. S. M. Pickard and B. Derby, *Mater. Sci. Engng* **A135,** 213 (1991).
31. Y. C. Chen and G. S. Daehn, *Metall. Trans.* **22A,** 1113 (1991).
32. H. Zhang, G. S. Daehn and R. H. Wagoner, *Scripta metall. mater.* **24,** 2151 (1990).
33. M. Y. Wu and O. D. Sherby, *Scripta metall.* **18,** 773 (1984).
34. S. H. Hong, O. D. Sherby, A. P. Divecha, S. D. Karmarkar and B. A. McDonald, *J. Comp. Mater.* **22,** 102 (1988).
35. H. Zhang, G. S. Daehn and R. H. Wagoner, *Scripta metall. mater.* **25,** 2285 (1991).
36. G. S. Daehn and T. Oyama, *Scripta metall. mater.* **22,** 1097 (1988).
37. G. S. Daehn and G. Gonzalez-Doncel, *Metall. Trans.* **20A,** 2355 (1989).
38. G. S. Daehn, ASTM SP 1080, p. 70. ASTM, Philadelphia, PA (1990).
39. Y. C. Chen, G. S. Daehn and R. H. Wagoner, *Scripta metall. mater.* **24,** 2157 (1990).
40. G. Gonzalez-Doncel, S. D. Karmarkar, A. P. Divecha and O. D. Sherby, *Composites Sci. Technol.* **35,** 105 (1989).
41. D. Toitot, E. Andrieu and P. Jarry, *Metal Matrix Composites—Processing, Microstructure and Properties* (edited by N. Hansen, D. Juul-Jensen, T. Leffers, H. Lilholt, T. Lorentzen, A. S. Pedersen, O. B. Pedersen and B. Ralph), p. 695. Risø National Laboratory, Roskilde, Denmark (1991).
42. J. A. G. Furness and T. W. Clyne, *Metal Matrix Composites—Processing, Microstructure and Properties* (edited by N. Hansen, D. Juul-Jensen, T. Leffers, H. Lilholt, T. Lorentzen, A. S. Pedersen, O. B. Pedersen and B. Ralph), p. 349. Risø National Laboratory, Roskilde, Denmark (1991).
43. J. A. G. Furness and T. W. Clyne, *Mater. Sci. Engng* **A141,** 199 (1991).
44. M. L. Dunn and M. Taya, *Scripta metall. mater.* **27,** 1349 (1992).
45. B. Derby, *Scripta metall.* **19,** 703 (1985).
46. T. Ghorbel and D. Valentin, *Developments in the Science and Technology of Composite Materials, ECCM5* (edited by A. R. Bunsell, J. F. Jamet and A. Massiah), p. 735. European Association for Composite Materials (1992).
47. G. S. Daehn, *Scripta metall. mater.* **23,** 247 (1989).
48. F. H. Gordon and T. W. Clyne, *Residual Stresses in Composites: Measurement Modeling and Effects on Thermomechanical Behavior* (edited by E. V. Barrera and I. Dutta), p. 293. TMS, Warrendale, PA (1993).
49. K. Wakashima, B. H. Choi and S. H. Lee, *Japan–U.S. CCM—III* (edited by K. Kawata, S. Umekawa and A. Kobayashi), p. 579. Japan Society for Composite Materials (1986).
50. K. Wakashima, H. Tsukamoto and B. H. Choi, *Metal Matrix Composites—Processing, Microstructure and Properties* (edited by N. Hansen, D. Juul-Jensen, T. Leffers, H. Lilholt, T. Lorentzen, A. S. Pedersen, O. B. Pedersen and B. Ralph), p. 349. Risø National Laboratory, Roskilde, Denmark (1991).
51. C. M. Bedell, M.Sc. thesis, Massachusetts Institute of Technology, Cambridge, MA (1993).
52. *ASM Handbook: Alloy Phase Diagrams*, p. 2·25. ASM, Metals Park, OH (1992).
53. H. J. Frost and M. F. Ashby, *Deformation-mechanism Maps: The Plasticity and Creep of Metals and Ceramics*, p. 43, Pergamon Press, Oxford (1982).
54. J. Lunsford and N. J. Grant, *Trans. ASM* **49,** 328 (1957).
55. H. Oikawa, K. Nishimura and M. X. Cui, *Scripta metall.* **19,** 825 (1985).
56. H. E. McCoy, *Trans. ASM* **57,** 743 (1964).
57. J. J. Stobo, *J. Nucl. Mater.* **2,** 97 (1960).
58. Y. S. Touloukian, R. K. Kirby, R. E. Taylor and P. D. Desai, *Thermal Expansion: Metallic Elements and Alloys*. Plenum Press, New York (1975).
59. Y. S. Touloukian, R. K. Kirby, R. E. Taylor and P. D. Desai, *Thermal Expansion: Nonmetallic Solids*. Plenum Press, New York (1977).
60. I. Barin, O. Knacke and O. Kubaschewski, *Thermochemical Properties of Inorganic Substances (Supplement)*. Springer, Berlin (1977).
61. D. C. Dunand and C. M. Bedell, US Patent 5, 413, 649 (1995).
62. J. L. Hart and A. C. D. Chaklader, *Mater. Res. Bull.* **2,** 521 (1967).
63. C. A. Johnson, R. C. Bradt and J. H. Hoke, *J. Am. Ceram. Soc.* **58,** 37 (1975).
64. W. M. Kriven, *Solid–Solid Phase Transformations* (edited by H. I. Aaronson, D. E. Laughlin, R. F. Sekerka and C. M. Marvin), p. 1507. Metallurgical Society of AIME (1981).
65. D. A. Young, *Phase Diagrams of the Elements*. University of California Press, Berkeley, CA (1991).
66. E. M. Levin and H. F. McMurdie, *Phase Diagrams for Ceramists—1975 Supplement*, pp. 5–422. American Ceramic Society, Columbus, OH (1975).
67. S. H. White and R. J. Knipe, *J. Geol. Soc. Lond.* **135,** 513 (1978).
68. J. J. English and G. W. Powell, *Trans. AIME* **236,** 1467 (1966).
69. E. Sato and K. Kuribayashi, *Acta metall. mater.* **41,** 1759 (1993).
70. G. L. Povirk, S. R. Nutt and A. Needleman, *Scripta metall. mater.* **26,** 461 (1992).
71. J. D. Eshelby, *Proc. R. Soc. Lond.* **A241,** 376 (1957).

72. T. W. Clyne and P. J. Withers, *An Introduction to Metal Matrix Composites*, p. 44. Cambridge University Press, Cambridge, MA (1993).
73. P. J. Withers, G. Cecil and T. W. Clyne, *Proc. 2nd Eur. Conf. Adv. Mater. Proc.* (edited by T. W. Clyne and P. J. Withers), p. 134. The Institute of Metals, London, U.K. (1992).
74. Y. C. Chen and G. S. Daehn, *Scripta metall. mater.* **25,** 1543 (1991).

APPENDIX

Composite Transformation-Mismatch Superplasticity Model Using Biased Internal Strains

Daehn [38] considered the biasing of internal CTE-mismatch strains between an elastic, perfectly plastic matrix and aligned long fibers, and derived an expression for the strain $\Delta\epsilon_p$ resulting from a biasing external stress σ after half a thermal cycle:

$$\Delta\epsilon_p = \frac{3\cdot(1-f)}{2\cdot F^2}\epsilon_{mis}\frac{\sigma}{\sigma_0} \tag{A1}$$

where σ_0 is the matrix yield stress at the end of the half cycle, f is the fiber volume fraction and $F = L/4S$ is a geometric factor containing the fiber length L and the fiber spacing S. The mismatch strain is:

$$\epsilon_{mis} = \Delta\alpha(\Delta T - \Delta T_{crit}) \tag{A2}$$

where $\Delta\alpha$ is the CTE-mismatch between the two phases, ΔT is the magnitude of the temperature excursion and ΔT_{crit} is the temperature change needed to initiate matrix plasticity. While equation (A2) is strictly valid only for metal matrix composites containing long fibers, Chen and Daehn [74] found that, if the geometric factor F in equation (A1) is set equal to unity, good agreement is obtained with data for CTE-mismatch superplasticity in particulate-reinforced composites. For the case of a mismatch resulting from a change of matrix density upon transformation, we replace the thermal mismatch strain given in equation (A2) by:

$$\epsilon_{mis} = \left|\frac{1}{3}\frac{\Delta V}{V}\right| - |\Delta\alpha\Delta T| \tag{A3}$$

where the CTE contribution is subtracted from the uniaxial transformation strain, since the two mismatches are of opposite signs. We have thus assumed that the mismatch within the materials is completely relaxed at the upper and lower temperatures of the cycle.

We do not consider a critical strain for the onset of plasticity [corresponding to ΔT_{crit} in equation (A2)], since the matrix is assumed to be at the yield point as a result of the transformation-induced plasticity taking place independently of the reinforcement. Introducing equation (A3) and $F = 1$ into equation (A1) gives for a full cycle:

$$\Delta\epsilon_p = \frac{3\cdot(1-f)}{2}\cdot\left(\left|\frac{1}{3}\frac{\Delta V}{V}\right| - |\Delta\alpha\cdot\Delta T|\right)\cdot\left(\frac{1}{\sigma_{0\alpha}} + \frac{1}{\sigma_{0\beta}}\right)\sigma \tag{A4}$$

where $\sigma_{0\alpha}$ and $\sigma_{0\beta}$ are the yield stress of the sample, assumed to be fully α at 830°C at the end of the cooling period and fully β at 1010°C at the end of the heating period. As described earlier, we take for the yield stress the flow stress $\sigma(\dot{\epsilon}^*)$, given by equation (1), where $\dot{\epsilon}^* = 10^{-5}$ s^{-1}, resulting in $\sigma_{0\alpha} = 6.9$ MPa and $\sigma_{0\beta} = 1.34$ MPa. With the materials data given in the main body of the text, equation (A4) yields $\Delta\epsilon_p = 1.7$ GPa^{-1}, in approximate agreement with the observed value $\Delta\epsilon/\sigma$(Ti–TiC) − $\Delta\epsilon/\sigma$(CP–Ti) = 3 ± 1 GPa^{-1} (Fig. 8).